Publications of the Astronomical Society of the Pacific
107: 265–272, 1995 March

Measuring Astronomical Seeing: The DA/IAC DIMM

JEAN VERNIN

Département d'Astrophysique de l'Université de Nice, U.R.A. 709 du C.N.R.S., F-06108 Nice Cedex 2, France
Electronic mail: vernin@a]yalga.unice.fr

CASIANA MUÑOZ-TUÑÓN

Instituto de Astrofísica de Canarias, E-38200 La Laguna, Tenerife, Spain
Electronic mail: cmt@iac.es

Received 1994 June 6; accepted 1994 December 13

ABSTRACT. Accurate, absolute, and reproducible measurements are the expected qualities of any instrument. A differential image motion monitor (DIMM) is presented which assesses astronomical *seeing* with those requirements. It has been designed (with collaboration of the staff of the Département d'Astrophysique de l'Université de Nice and the Instituto de Astrofísica de Canarias: DA/IAC) also to be reliable, simple, transportable, and easy to set up, operate, and maintain. Its accuracy has been studied, both from theoretical and experimental points of view, mainly with respect to CCD sampling, photon noise, and threshold influence on centroid determination. The DA/IAC DIMM has been cross calibrated with the existing ESO DIMM. It monitors the seeing with a temporal resolution better than half a minute. This type of instrument is essential for testing new and already existing sites and to ascertain that the surroundings of telescopes do not generate additional turbulence. It is also indispensable to optimize astronomical instrument selection in "flexible scheduling."

1. INTRODUCTION

As predicted by diffraction theory, when light propagates in a homogeneous medium, the image of a point source produced by a telescope of diameter D, at a given wavelength λ, is an Airy spot of size $\varepsilon_D \sim \lambda/D$. But turbulence degrades astronomical images and, prior to reaching the entrance pupil of a telescope, light coming from a star crosses several turbulent atmospheric layers which perturb the beam propagation. For this reason, at the telescope focus, it is impossible to reach the theoretical angular resolution ε_D of a perfect mirror. The star image is degraded in such a way that its size depends mostly on the turbulence integrated throughout the atmosphere, being almost insensitive to telescope diameter. The traditional way to characterize image degradation in astronomy is to measure the full width at half-maximum intensity $\varepsilon_{\mathrm{FWHM}}$ of a star at the focus of a telescope.

According to Fried's theory (1966), image degradation produced by atmospheric turbulence is characterized by the so-called r_0 parameter. This r_0 can be imagined as the telescope diameter that would produce a diffraction spot of the same size as that produced by the atmospheric turbulence on a point source observed with an infinite mirror.

With formal analogy to the expression relating those parameters for pure diffraction images, the relationship between $\varepsilon_{\mathrm{FWHM}}$ and r_0 can be written as

$$\varepsilon_{\mathrm{FWHM}} = 0.98\frac{\lambda}{r_0} \qquad (1)$$

for $r_0 \ll D$.

What we call seeing in astronomy is the angular diameter $\varepsilon_{\mathrm{FWHM}}$ of a star image (generally expressed in units of arcsecond) at the focus of a large-diameter telescope and taken with long exposure. It is important to bear in mind that seeing includes the "blurring," or instantaneous image broadening, and the "image motion" or erratic displacement of the image.

Importance of the problem. For the new-generation 8-m telescopes and a typical 10 cm r_0 value, the "degradation" ratio $D/r_0 = 8/0.1 = 80$ is of extreme importance. It has many repercussions in different fields of astronomy such as photometry, classical imaging, spectroscopy, or high-angular resolution (HAR) (Dennefeld and Fort 1986; di Serego Alighieri 1986; Roddier and Lena 1984). In speckle interferometry, for instance, for a given angular frequency cutoff, ε is more important than D as far as the limiting magnitude is concerned.

Because of the cost of large-diameter telescopes and for increasingly sophisticated HAR imaging techniques, it is of the highest priority to assess the ultimate seeing of new and already existing sites. The main reasons are to select the best locations, to design the most suitable instrumental techniques, and to be sure that already existing telescopes are not affected by man-made turbulence. Since seeing varies significantly with time, turbulent conditions need to be evaluated quantitatively to optimize the type of instrument working at the focus of a telescope. A seeing monitor is thus required to implement "flexible scheduling."

History. Many different attempts have been made to measure seeing since the pioneering work by Rösch (1963). Although the parameters relevant to image degradation are related to geophysics (turbulent fluctuations of air density), all seeing monitors (SM) are optical instruments; balloon data (Vernin and Muñoz-Tuñón, 1992, 1994) can be used to estimate $\varepsilon_{\mathrm{FWHM}}$ but cannot monitor it versus time. Different concepts have been used: Danjon method, Polaris trail, shearing interferometer (Roddier 1976), Scidar technique (Azouit and Vernin 1980), differential image motion monitor (DIMM) (Stock and Keller 1960; Sarazin and Roddier 1990), and grating scale monitor (GSM) (Martin et al. 1994). They use different receivers such as the eye, photographic plates, photomultipliers, or intensified CCDs.

Problems. Although recent instruments, such as shearing

interferometer, GSM, and DIMM are based on sound theory and are able to give quantitative measurements, all of them are prototypes and have been used independently, with very few cross calibrations. Telescope instrumentation is now so expensive that it is mandatory to have access to calibrated seeing and to choose an improved technique, which can be easily installed all over the world, given absolute, reliable, and accurate values.

Solution. In 1989 the authors decided to build this "standard instrument." It was funded and developed within the framework of a site assessment at the Observatorio del Roque de los Muchachos (ORM) at La Palma, directed towards an 8 m telescope project. We have benefitted from the experience of the VLT working group and from the paper by Sarazin and Roddier (1990) describing the ESO DIMM. The instrument was designed to be transportable, reliable, cost effective, easy to handle, documented and calibrated, and easily duplicated. To us these are the requirements for an universal instrument to measure seeing.

In Sec. 2 we will give a detailed description of the DA/IAC DIMM (Département d'Astrophysique and the Instituto de Astrofísica de Canarias) underlining the differences from the ESO DIMM.

Sections 3 and 4 are dedicated to a theoretical study of the influence of threshold and photon noise in data processing as well as to a numerical simulation and experimental verification of these topics. The results of a cross-calibration campaign in Chile between both (ESO and DA/IAC) DIMMs, while working together at mount Paranal, are given in Sec. 5. Finally in Sec. 6 we will indicate whether or not our goals are fulfilled.

2. SEEING MONITOR DESCRIPTION

The DA/IAC DIMM was conceived as an instrument very similar to the ESO DIMM, with the same physical basis, but transformed to become a commercial product satisfying the above-mentioned requirements.

2.1 Summary of Optical Fundamentals

To estimate Fried's parameter r_0, one can measure the variance of the two-dimensional image position through a single aperture of diameter D

$$\sigma^2=0.373\varepsilon^2_{\mathrm{FWHM}}\left(\frac{r_0}{D}\right)^{1/3}. \tag{2}$$

One can imagine that, measuring image motion at the focus of a telescope with known aperture D and wavelength λ, the Fried's parameter and hence the seeing can be deduced from Eq. (1). This technique has extensively been used but requires a very stiff (and thus massive) telescope because image motions due to turbulence and to vibration cannot be separated. The variance obtained $\sigma^2_{\mathrm{total}}$ is the quadratic sum of two terms, one related to turbulence itself σ^2_{turb} and the other $\sigma^2_{\mathrm{telescope}}$ which includes the guiding, wind shaking, and dome effect

$$\sigma^2_{\mathrm{total}}=\sigma^2_{\mathrm{turb}}+\sigma^2_{\mathrm{telescope}}. \tag{3}$$

The DIMM principle is to produce twin images of a star, with the same telescope via two entrance pupils separated by a distance d. The differential method eliminates erratic motion of the telescope, measuring the angular differences over two small pupils d apart. The knowledge of the phase structure function, which is assumed to result from a Kolmogorovian behavior of the turbulence, enables us to assess the longitudinal and transverse (parallel and perpendicular to aperture alignment) variance of differential image motion as given by

$$\sigma^2_{l/t}=\sigma^2[1-k(l/t)(D/d)^{1/3}] \tag{4}$$

with

$$k(l)=0.541 \quad \text{and} \quad k(t)=0.810 \tag{5}$$

which holds when $D/d\leqslant 0.5$ (Sarazin and Roddier 1990, and references therein).

From those two expressions, two independent r_0 values are obtained which, in principle, should have the same value. As pointed out by Sarazin and Roddier (1990), recording both values is useful not only to improve the statistical estimate but also to be sure that no temporal smoothing is affecting the measurements. As discussed by Martin (1987), under very unfavorable wind conditions (strong wind gusts), due to the finite exposure time, the results provided by the differential image technique may be affected by errors. As a result the seeing values obtained in the longitudinal and transverse directions are different. Recording both values is the only way to be sure one is working under the conditions of applicability of the differential technique.

Formulas (2), (4), and (5) rely on the assumption that turbulence behaves according to Kolmogorov description. If it is not the case, these expressions are completely different, as shown by Fuchs et al. (1994). Here, a classical Kolmogorov turbulence is supposed, because measurements made for a single distance d cannot allow us to determine whether the above-mentioned hypothesis is true or false.

2.2 Mechanical and Optical Design

Compared to ESO DIMM, simpler solutions have been chosen in terms of optical and mechanical systems. The main differences are as follows.

(1) Instead of reimaging the pupil plane, the diaphragms and the small-angle deviation wedge have been located on a mask attached to the telescope entrance pupil. The optical system is then simpler, less sensitive to aberration, and easier to maintain.
(2) To match the pixel size, the focal length is increased using a simple eye piece. The equivalent ESO DIMM focal length is 5.25 m, but ours is 7.3 m.
(3) The intensified CCD camera is provided with an adjustable electronic shutter instead of a mechanical shutter to avoid temporal convolution.
(4) Tracking is with a stiff classical equatorial mount instead of an alt-azimuth mount.

Most of the items for the DA/IAC DIMM are found "over the counter" such as the 8 in. (20 cm) Celestron telescope,

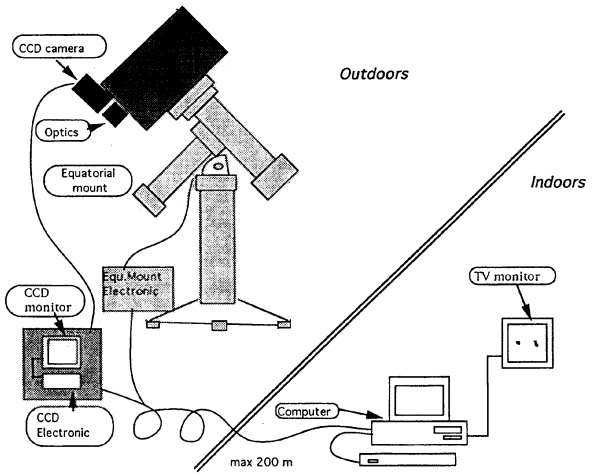

FIG. 1—General scheme of the DA/IAC DIMM.

the Basellga equatorial mount (which is provided with slow slew motion to allow automatic tracking), the pulsed intensified CCD LHESA camera, and the image-capture MATROX device that resides in a PC-AT computer. In Fig. 1 a schematic of the DA/IAC DIMM is presented. A few items have to be ordered specially like the optical wedge, the entrance diaphragm, and some mechanical pieces to attach the camera and the eye piece to the telescope.

2.3 Data Processing

Different authors (Sarazin and Roddier 1990; Martin 1987) have pointed out that short exposure time is very critical to reduce temporal blurring. The ESO DIMM uses 10-ms exposure time. But during short periods, corresponding to unusually high wind speed, it becomes necessary to reduce the exposure time until longitudinal and transverse seeing reaches the same value. This is why we have used an adjustable shutter speed, variable from 1 to 10 ms which allows us to increase the dynamic range of the instrument. Another problem could appear as a result of remanent images due to the decay time of the phosphor screen at the output of the intensifier. This might blur consecutive images leading to bias in seeing measurements as well as exposure time. With the intensified CCD camera used (P20 phosphor), 20 ms after a short exposure only 1/15 of the incident flux remains from the previous frame. We thus opted for opening the shutter at the frame rate (25 images/s, i.e., every 40 ms) assuming that a $(1/15)^2$ blur introduces a negligible effect in the derived seeing value.

The electronic shutter, which commands the high voltage of the microchannel plate of the intensifier, triggers 25 exposures per second, and images captured by the sampling board are made of two interleaved frames. One corresponds to the shutter opened while the other corresponds to a dark frame. Those two images are sent to the computer and are separated by software. In order to save time in frame transfer from the image acquisition board to the computer, two small windows on the CCD are selected, containing the two separated images of the star. The size of both windows can be chosen so as to match the image motion amplitude, related to seeing value.

Within each window the relative position of the stellar patch is computed along both x and y directions using a simple barycenter algorithm. The position of each window is known precisely and thus, locating the centroid of the spot (star), the absolute position of both star images is recorded in the computer memory.

Images in which any one of the centroids is too close to the border of the windows are rejected. The position of the last five centroids are kept in memory and then a linear regression is applied to predict the next position of the star in the focal plane, so as to relocate the windows. This feature is very convenient to follow slow image motion induced by tracking errors and minimizes the number of rejected images. When the star images cross some predefined boundary close to the CCD edge, the acquisition process is stopped, the corresponding slew motor is switched on to recenter the star, then a whole frame is grabbed to determine the new positions of both stars and the measurement procedure starts again.

After a given number of consecutive images have been captured (say 200) and the centroid positions recorded, the seeing is computed through Eqs. (4) and (5). Other parameters are also computed and recorded such as: the average x and y widths of stellar patches (to discard data affected by possible mechanical vibration or optical misalignment), the average flux of each star, and the scintillation index. Under reasonably good conditions (no rejected images and small windows) it is possible to monitor the seeing with a temporal sampling rate of less than half a minute.

2.4 Setting Up the Seeing Monitor

Once the seeing monitor has been installed on its site, it is necessary to perform the standard setting of an equatorial mount and to verify that each optical part is well aligned. Then, in order to initiate the measurements, the observer needs to select a known star and point the instrument, check that the star is within the CCD field, run the program to adjust the gain of the image intensifier, and start. The coordinates of the source are used to make the correction for air mass. Everything is thereafter under control of the computer for several hours. All relevant parameters are displayed on the computer screen as well as the positions of the two windows and the centroids of the two stars which are superimposed on the video monitor. The information, σ_l, σ_t, FWHM, flux, and scintillation index is automatically recorded on the computer disk. A sketch of the whole instrument setup is presented in Fig. 2. As seen in the figure, the maximum recommended distance between the outdoor part of the instrument and the data acquisition block is about 200 m.

2.5 Technical Parameters

The most relevant parameters which have been chosen in the design and construction of the DA/IAC DIMM are as follows.

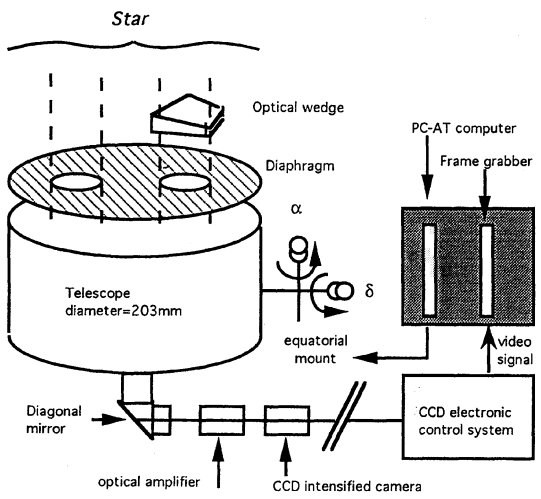

FIG. 2—General configuration and components of the DA/IAC DIMM.

(i) *Optical and geometrical parameters.*
Telescope type: 8" (20 cm) Schmidt—Cassegrain (Celestron),
telescope diameter: 203 mm,
telescope focal length: 2000 mm,
twin pupil diameter: 60 mm,
distance between pupils: 140 mm,
equivalent focal length: 7300 mm,
prism deviation angle: ~30 arcsec.

(ii) *Intensified CCD camera.*
LH-5038 (LHESA—Electronique) with fiber optical coupling to CCD (demagnification 1:1.5),
photocathode: S20R,
phosphor: P20,
shutter exposure time: Variable from 1 to 10 ms,
CCD pixel number: 576(V)×550(H),
pixel size: 23(V)×23(H) μm.

(iii) *Video image grabber board: PIP 1024 (Matrox).*
Video acquisition is not synchronized with CCD pixel readout. Matrox pixel size at image intensifier entrance window: 24.5×33.4 μm.

(iv) *Equatorial mount: MT 3 (Basellga).*
No automatic pointing,
automatic guiding.

(v) *Computer: PC-AT.*

3. CCD NOISE AND THRESHOLD INFLUENCE

Among the possible techniques to compute the centroid position we used the barycenter method which requires the dark field to have a zero mean. Otherwise the computed centroid is viciated by the position of the "platform" on which the star image is superimposed. Further, the sampled dark field can be regarded as a source of noise which increases the uncertainty of the centroid with the window size, when compared to the finite energy of the star flux.

From each window two profiles $I(x)$ and $I(y)$ are computed. $I(x)$ being an integration along y and $I(y)$ along x. The position of the centroid along the x axis, as given by the barycenter theorem, is

$$X=\frac{\int_a^b xI(x)dx}{\int_a^b I(x)dx}, \tag{6}$$

a and b being the edges of the window. If a dark noise with zero-mean $N(x)$ is added to star intensity, one can write the position of the centroid of the contaminated (measured) signal X_m as

$$X_m=\frac{\int_a^b x[I(x)+N(x)]dx}{\int_a^b [I(x)+N(x)]dx} \tag{7}$$

but taking into account that noise is centered

$$X_m=X+\frac{\int_a^b xN(x)dx}{\int_a^b I(x)dx}=X+X_N. \tag{8}$$

In addition to photon noise, there are several other sources of noise when working with a CCD, i.e., readout, dark current, and sampling noises, which influence the measurement of the centroid position.

As demonstrated by Gely (1994), due to CCD noise, the variance σ_x^2 of the centroid position in x direction and in the absence of photon noise is given by

$$\sigma_x^2=\frac{M^2(M^2-1)\Delta x^2\sigma_{\mathrm{CCD}}^2}{12I^2}, \tag{9}$$

where M is the lateral size of the sampled window ($M\times M$) in pixel units, Δx is the width of the pixel, σ_{CCD}^2 is the estimated (dark-current, sampling, and readout) noise of the CCD receiver, and I is the mean flux of the star, being $I=\sum_{i=1}^{M} I_i$. It should be noted that the centroid position error grows with the fourth power of the window size and decreases as the total flux increases. This assumption has been experimentally tested and the results are plotted in Fig. 3, where the variance (markers) of the measured centroid of a point source is given versus the size of the window M. The theoretical curve (solid line), given in Eq. (9) is also represented.

In order to avoid centroid position error deterioration as the size of the window increases (e.g., during bad seeing conditions) the idea of using a threshold is rather tempting. Outside the star boundary, the window is filled with zeros and σ_x^2 becomes independent of M, but, conversely part of the stellar flux is lost. The way to proceed in order to avoid an amplification of the errors has to be carefully chosen. We have investigated this problem both via numerical simulations and experimental measurements.

Laboratory simulation. In order to test the threshold effect on barycenter position we used an already existing laboratory experiment consisting of an afocal light beam in which a turbulent layer is introduced. The turbulent flow is controlled by the mixing of two flows with different density (temperature) and speed (Fuchs et al. 1994). A lens simulates

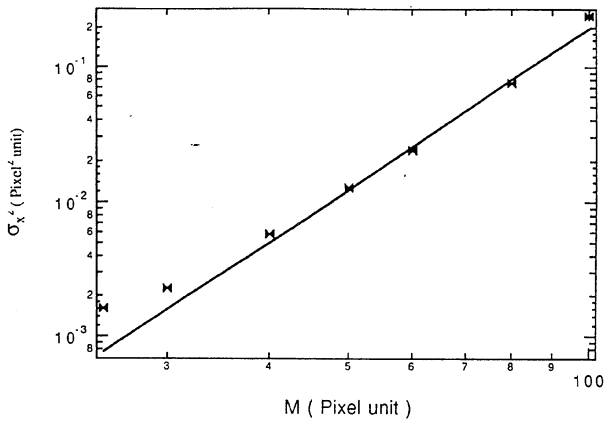

FIG. 3—Influence of the window size M on estimation error of centroid position σ_x^2. Markers refer to experimental measurements while the solid line is a fit, assuming a $M^2(M^2-1)$ behavior.

the entrance pupil of a telescope, on which two diaphragms are placed to follow the DIMM principle. An algorithm computes the centroid of the stellar patch using a threshold that varies between zero and a value corresponding to half of that measured in the brightest pixel. The zero ground level is computed from those pixels assumed to be out of the stellar patch.

Numerical simulation. In order to compare the experimental results obtained in the laboratory, a one-dimensional wave-front simulator was used (Sánchez and Petrov 1994). The algorithm for the simulation assumes a Kolmogorovian behavior of the turbulence. The corrugated wave front passes through the circular aperture of a lens and at its focus the stellar patch is computed and the centroid position is calculated.

Both experimental and simulated seeing are plotted in Fig. 4 as a function of the threshold and for different values of D/r_0. In Fig. 4(a), the behavior of the estimated seeing is sketched for three different levels of turbulence and for four thresholds. The ordinates are labeled in arbitrary units of σ_x^2 because the generated turbulence has nothing to do with a Kolmogorov trend. It is clear that, as turbulence and threshold increase, overestimation of the seeing becomes more serious. In Fig. 4(b), simulated wave fronts are generated for various r_0 ranging from 4 to 20 cm, then passing through a 6 cm aperture. Plotted seeing is normalized by that obtained without any threshold. One notes that, as soon as a small threshold is set, the seeing is overestimated. As expected, this spurious effect is worst when turbulence as well as threshold increase. But, even when $r_0 \gg D$, where one would expect a pure Airy disk without any threshold effect, the seeing is still contaminated.

4. PHOTON NOISE INFLUENCE

Goad et al. (1986) analyzed the variance of the position of the centroid of a Gaussian-shape star in presence of photon noise. Let σ_s be the Gaussian width of the star. They found that, provided a sufficiently large number of pixels sample

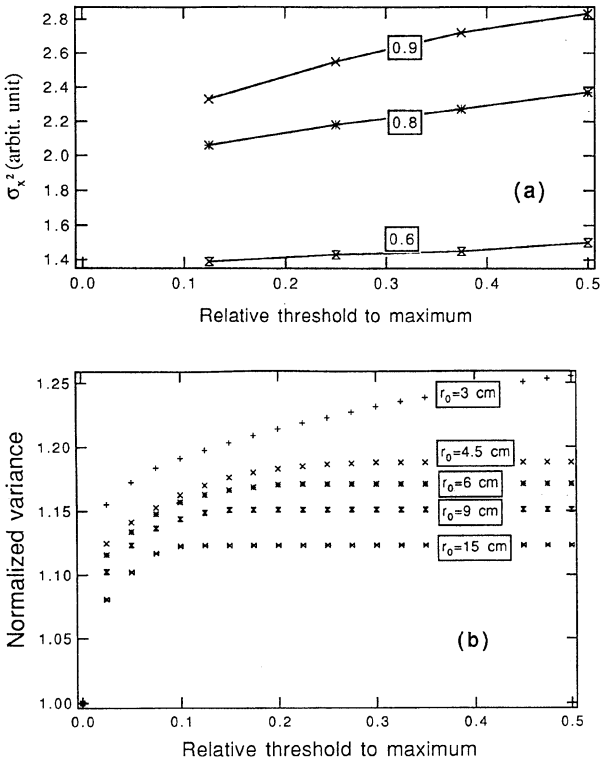

FIG. 4—Influence of the threshold and the D/r_0 ratio (encapsulated numbers) on seeing assessment. (a) Results from laboratory experimental measurements, (b) numerical simulation.

the stellar patch (i.e., $\Delta x < \sigma_s/4$), the variance of the centroid position error is given by

$$\sigma_x^2 = \frac{\pi \sigma_s^2}{2N}, \tag{10}$$

where N is the photon number in each image for which the centroid is computed. Expression (10) is written in pixel units ($\Delta x = 1$).

Under the same conditions, Gely's analysis (1994) yields a similar, but more detailed, expression

$$\sigma_x^2 = \frac{M^2(M^2-1)\sigma_{\mathrm{CCD}}^2}{12I^2} + \frac{1}{N}\left(\sigma_s^2 + \frac{1}{12}\right) + \epsilon. \tag{11}$$

The first term of the right-hand part of this formula takes into account the CCD noise influence, already discussed in the previous section, whereas ϵ is a term that becomes as small as we wish when the star patch is oversampled. As stated in Sec. 3, the first term in Eq. (11) can also be neglected when a threshold is used.

Both of the above-mentioned authors assumed a perfect impulse response of the photoelectric receiver. Our DA/IAC DIMM, as many other instruments, uses an image intensifier which makes a convolution to amplify the intensity of the stellar source. For simplicity let us suppose that the impulse response function of the image intensifier has a Gaussian shape of width σ_{ii}, then it can be written

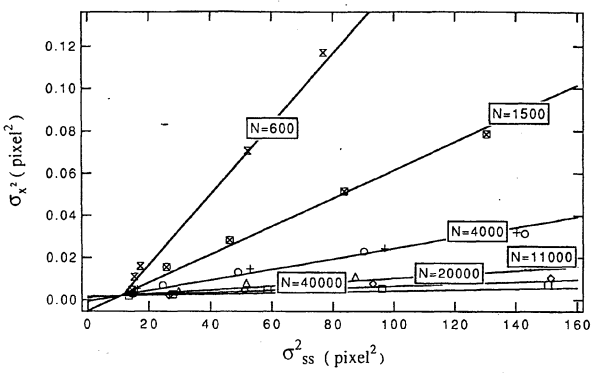

FIG. 5—Additive bias introduced by photon noise in seeing assessment. Variance in the centroid position σ_x^2 is measured in a laboratory experiment as a function of the size σ_{ss}^2 of the source at the CCD entrance window and for different light fluxes expressed in photon number N. N has been deduced from formula (20) to fit the experimental data. No turbulence is introduced in the light beam.

$$\sigma_{ss}^2=\sigma_s^2+\sigma_{ii}^2, \tag{12}$$

where σ_{ss} is the width of the image of the star sampled by the CCD which reads out the phosphor screen of the image intensifier. This leads to a simplified expression of Eq. (11) as

$$\sigma_x^2=\frac{1}{N}\left(\sigma_{ss}^2-\sigma_{ii}^2+\frac{1}{12}\right). \tag{13}$$

In Fig. 5, the experimental centroid position variance (markers) σ_x^2 versus σ_{ss}^2 for various photon number N is plotted. Solid lines try to fit these measurements according to expression (13), adjusting N, the photon number. Taking into account that, in the absence of photon noise, the minimum measured CCD noise is about 2×10^{-3} pixels^2, the set of curves in Fig. 5 clearly shows that Eq. (10) or Eq. (13) is verified if it is assumed that σ_{ii}^2 is about 11 pixels^2 (i.e., $\sigma_{ii}=3.3$ pixels); this is the value towards which all lines converge. Since our CCD pixel size in x is 24.5×10^{-6} m, the impulse response width of the image intensifier is $\sim$81 μm, which is a commonly found value.

The straight-line set plotted in Fig. 5 follows the relation

$$\sigma_x^2=2\times10^{-3}+\frac{1}{N}(\sigma_{ss}^2-11). \tag{14}$$

Theory and experience seem to agree, enabling us to remove this noise if one knows N, from the magnitude of the tracked star. Assuming that 10^6 photons are received on 1 cm^2, within a $\Delta\lambda=0.1$ μm, each second from a star of magnitude $m_v=0$, it is easy to express N:

$$N=43\times10^5\Delta T10^{-m_v/2.5} \tag{15}$$

as a function of m_v, and ΔT the time exposure. The bandwidth of our image intensifier is about 0.4 μm with a mean quantum efficiency of 5%. The atmosphere and telescope transmission is estimated to be 0.5.

Taking into account the already detailed DA/IAC DIMM parameters (refer to Sec. 2.5), and assuming $\lambda=0.5\times10^{-6}$ m, one finds that the longitudinal and transverse seeings depend

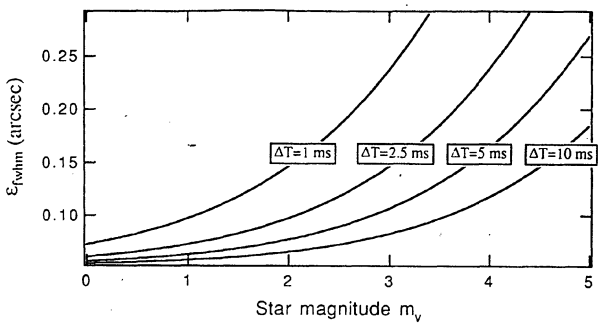

FIG. 6—Seeing bias vs star magnitude for different time exposure (box) and for most of the DA/IAC DIMM working conditions.

on the longitudinal and transverse rms of the centroid position in x and y directions, i.e., σ_x and σ_y

$$\varepsilon_{\text{FHWM }l}=6.96\times10^{-6}\sigma_x^{6/5}, \tag{16}$$

$$\varepsilon_{\text{FHWM }t}=13.0\times10^{-6}\sigma_y^{6/5}. \tag{17}$$

Formulas (14) and (15) can be substituted into Eqs. (16) and (17) to assess the seeing bias

$$\varepsilon_{\text{seeing bias}}=10.5\times10^{-6}\left(\sigma^2_{\text{sampling}}+\frac{\sigma_s^2}{43\times10^5\Delta T10^{-m_v/2.5}}\right)^{3/5}. \tag{18}$$

In formula (18) we took in account that DIMM is a differential technique in which the variance of the position difference of the two stellar patches is computed, leading us to introduce a $2^{3/5}$ factor. If one assumes that most of the time, the Fried's parameter r_0 is larger than the entrance pupil D of the DIMM, the focal patch size is close to $\lambda f/D$. Thus $\sigma_s^2\sim(\lambda f/D\Delta x)^2$ which is of the order of 6.2 pixels^2. Taking $\sigma^2_{\text{sampling}}\sim2.10^{-3}$, one can evaluate the bias seeing as a function of the star magnitude, for different time exposure, as shown in Fig. 6. From this figure, it is clear that, if a 0.1 arcsec seeing error is acceptable, no photon noise correction is required for a star brighter than magnitude 3.5 ($\Delta T=10$ ms) or 2 ($\Delta T=2.5$ ms). Moreover, as the whole set of relevant parameters is known in real time during the measurements, it is possible to cancel out this spurious seeing.

5. CALIBRATION

Pedersen et al. (1988) compared the ESO DIMM with seeing measured at the focus of a large telescope and found a correlation coefficient of 0.97. This agreement shows that both instruments were well calibrated and that Kolmogorov theory is applicable through expressions (2) and (4).

A comparison was performed between the ESO DIMM and the DA/IAC DIMM during the Paranal Seeing Campaign which was held during March and April 1992. Both DIMMs were simultaneously operated on the same site close to the Cerro Paranal (altitude: 2600 m, latitude: 24° 37′ S, longitude: 70° 24′ W) which is the site selected to install the European Southern Observatory Very Large Telescope. In

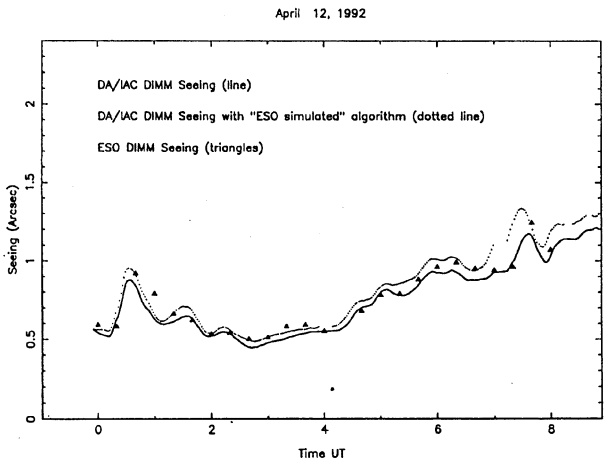

FIG. 7—Seeing values (Paranal—Chile) in arcsec vs. UT time. Comparison between ESO DIMM (black triangles), DA/IAC DIMM (continuous line) and "ESO Simulated" with DA/IAC DIMM (dotted line), for the night of 1992 April 12.

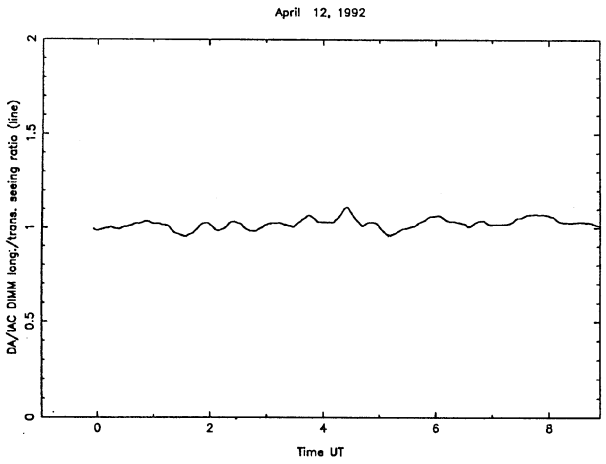

FIG. 8—Transverse to longitudinal seeing ratio vs. time for the same night of 1992 April 12.

Fig. 7 seeing measured by ESO DIMM (triangles) and DA/IAC DIMM (continuous line) is plotted versus time for one of the nights of the Paranal campaign. One can see a bias, ESO seeing values being slightly larger than the DA/IAC ones most of the time. This discrepancy can be interpreted in terms of threshold influence as already shown in Sec. 3. The algorithm used in the ESO DIMM to determine the centroid algorithm defines a threshold of half the intensity measured on the brightest pixel, whereas our DIMM (DA/IAC) sets the cutoff level just above the dark noise level of the camera.

In order to take this into account and also for coordination with the Paranal campaign, we simulated the ESO's algorithm with DA/IAC DIMM; we switched between the ESO and DA/IAC algorithm every 200 images and recorded both sets of measurements separately. In Fig. 7 "ESO simulated" (dotted line) data are plotted showing that ESO seeing (triangles) lie within both lines which correspond to both algorithms implemented on DA/IAC DIMM. In Fig. 8, the ratio between longitudinal and transverse seeing values (from DA/IAC DIMM) are given versus time. This ratio being always around unity ensures the reliability of the measurements, discarding any temporal convolution.

For the reasons presented in Sec. 3 and according to Fig. 4 it seems more convenient to use an algorithm which takes into account most of the stellar profile in order to determine the centroid. Sampling the upper part of the profile, although a good approach in most cases, might introduce an error (more than 10%) in the determination of the seeing. This error is not easy to quantify and varies depending on S/N ratio and seeing conditions.

6. DA/IAC DIMM PERFORMANCE AND FINAL REMARKS

From Sec. 4, the DA/IAC DIMM achieves an accuracy better than 0.1 arcsec for stars brighter than fourth magnitude and a 10-ms time exposure. Remembering the fact (Vernin and Muñoz-Tuñón 1992) that seeing may on *no account* be summed linearly, $\varepsilon_{\text{tot}}=(\Sigma_i \varepsilon_i^{5/3})^{3/5}$, a 0.1 arcsec error achieved on a 0.5 arcsec seeing leads to only a 4% relative error. Using a PC-AT 386 computer, a reliable seeing measurement is attained within less than half a minute, for 26×26 pixels sampled windows. The stiffness of the equatorial mount allowed us to get valid seeing measurements until the wind crosses a threshold of about 15 m/s. With a 10-ms time exposure the monitor gives accurate measurements, pointing at stars as faint as magnitude 3. If one wishes to avoid ground-surface turbulence contribution the monitor should be placed on top of an about 5 m tower (Vernin and Muñoz-Tuñón 1994).

Quantitative seeing measurements are given by differential image motion monitors according to a well-established theory and a concept which makes them insensitive to optical aberrations and wind shake of the instrument. In this paper we put emphasis on the simplicity and reliability of the DA/IAC DIMM. Great care has been taken to assess the influence of photon noise and threshold effects on centroid position variance. Some of our conclusions can be extended to astronomical fields where accurate metrology is necessary such as astrometry, fringe tracking, and Shack–Hartmann wave-front sensing.

The DA/IAC DIMM has been intensively used in many different sites such as Aire/Adour (France), Nice (France), Izaña (Tenerife, Canary Island, Spain), Paranal (Chile), and is working at this moment at the Observatorio del Roque de los Muchachos (La Palma, Canary Island, Spain). During those numerous displacements, the monitor appeared to be reliable and easy to handle thanks to the components it is made of. From our experience, this monitor can be set up and used under most astronomical conditions (high altitude, wind gusts, cold weather) and seems to resist most common human mishandling!

This work has been funded by the Instituto de Astrofísica de Canarias and the program for collaborative research between France and Spain. We are very grateful to Marc Sarazin for his support and valuable comments which were

mostly useful for the design of our instrument. It was a pleasure to have Sergio Hernandez working with us during a long and crucial period of the project. His work has been of decisive importance and is reflected in many points written in the paper. The long experience of Max Azouit in CCD and electronic in general has certainly made things much easier. We are very grateful to Leonardo Sánchez-Peniche for his help in wave-front simulation and to Michel Tallon for many discussions about photon noise and threshold influence. We appreciate arguments provided by Chris Coulman as well as his help in final text corrections. Finally we are grateful to our referee René Racine for very constructive and useful comments.

REFERENCES

Azouit, M., and Vernin, J. 1980, J. Atm. Sci. 37, 1550
Dennefeld, M., and Fort, B. 1986, ESO's Very Large Telescope, ed. D'Odorico and J. P. Swings, Venice (Garching), p. 151
de Serego Alighieri, S. 1986, ESO's Very Large Telescope, ed. D'Odorico and J. P. Swings, Venice (Garching), p. 173
Fried, D. L. 1966, JOSA, 56, 1372
Fuchs, A., Tallon, M., and Vernin, J. 1994, in Atmospheric Propagation and Remote Sensing III, Orlando, 5–7 April [Proc. SPIE 2222, 682]
Gely, F. 1994, Rapport de stage, Etoile Laser Polychromatique, Nice University
Goad, L., Roddier, F., Beckers, J., and Eisenhardt, P. 1986, in Advanced Technology Optical Telescopes III [Proc. SPIE 628, 305]
Martin, F., Tokovinin, A., Agabi, A., Borgnino, J., and Ziad, A. 1994, A&A (in press)
Martin, H. M. 1987, PASP, 99, 1360
Pedersen, H., Rigaut, F., and Sarazin, M. 1988, The Messenger, 53, 8
Roddier, C. 1976, J. Opt. Soc. Am., 66, 478
Roddier, F., and Lena, P. 1984, J. Optics (Paris), 15, 171
Rösch, J. 1963, Le Choix des Sites d'observatoires Astronomiques (site testing), IAU Symposium No. 19
Sánchez, L. J., and Petrov, R. G. 1994, Atm. Oceanic Opt. (in press)
Sarazin, M., and Roddier, F. 1990, A&A, 227, 294
Stock, J., and Keller, G. 1960, in Stars and Stellar Systems, Vol. 1, ed. G. P. Kuiper and B. M. Middlehurst (Chicago, University of Chicago Press), p. 138
Vernin, J., and Muñoz-Tuñón, C. 1992, A&A, 257, 811
Vernin, J., and Muñoz-Tuñón, C. 1994, A&A, 284, 311